Journal of Medicinal Chemistry

pubs.acs.org/jmc

Article

Repositioning Food and Drug Administration-Approved Drugs for Inhibiting Biliverdin IXβ Reductase B as a Novel Thrombocytopenia Therapeutic Target

Myeongkyu Kim, Jung-Hye Ha, Joonhyeok Choi, Bo-Ram Kim, Vytautas Gapsys, Ko On Lee, Jun-Goo Jee, Kalyan S. Chakrabarti, Bert L. de Groot, Christian Griesinger,* Kyoung-Seok Ryu,* and Donghan Lee*

Cite This: J. Med. Chem. 2022, 65, 2548−2557

Read Online

ACCESS | Metrics & More | Article Recommendations | Supporting Information

ABSTRACT: Biliverdin IXβ reductase B (BLVRB) has recently been proposed as a novel therapeutic target for thrombocytopenia through its reactive oxygen species (ROS)-associated mechanism. Thus, we aim at repurposing drugs as new inhibitors of BLVRB. Based on IC_{50} (<5 μM), we have identified 20 compounds out of 1496 compounds from the Food and Drug Administration (FDA)-approved library and have clearly mapped their binding sites to the active site. Furthermore, we show the detailed BLVRB-binding modes and thermodynamic properties (ΔH, ΔS, and K_D) with nuclear magnetic resonance (NMR) and isothermal titration calorimetry together with complex structures of eight water-soluble compounds. We anticipate that the results will serve as a novel platform for further in-depth studies on BLVRB effects for related functions such as ROS accumulation and megakaryocyte differentiation, and ultimately treatments of platelet disorders.

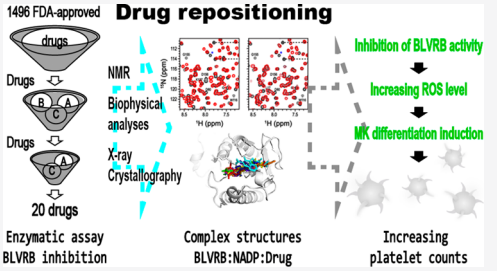

1. INTRODUCTION

Platelets (thrombocytes) are produced from megakaryocytes (MK) that are differentiated from a multipotent hematopoietic stem cell[1,2] and play important roles not only in blood hemostasis and pathological thrombosis but also in other biological processes, including inflammation, neo-angiogenesis, innate immunity, adaptive immune responses, and tumor metastasis.[3−5] Therefore, the regulation of platelet population and the control of specific platelet responses are prominent targets for new drugs against platelet disorders.[6] The impairment of platelet regulation leads to various bleeding disorders,[7,8] including thrombocytopenia, a familial genetic disorder, that is characterized by increased bleeding (hemophilia) due to low platelet counts.[9] A typical treatment intervention for thrombocytopenia is the increase in platelet counts by the induction of platelet generation[10] or platelet transfusion.[11] On the other hand, thrombocytosis is characterized by excessive platelets in the blood, as opposed to the symptom of thrombocytopenia,[12] Through the cohort analysis of thrombocytosis with large-scale platelet transcriptome sequencing in both primary (essential) and secondary (reactive) thrombocytosis cohorts, it was found that biliverdin reductase B (BLVRB) has an ability to control the production of platelets through MK differentiation by reactive oxygen species (ROS) control.[13,14]

In the heme degradation pathway, BLVRB reduces biliverdin (BV)-IXβ to bilirubin (BR)- IXβ by utilizing NAD(P)H in the downstream of heme oxygenase(s)-1 (inducible HMOX1) and -2 (constitutive HMOX2). The product of BLVRB, BR, is a potent antioxidant[15,16] and has an apparent cytoprotective effect,[17] although BR can be toxic at high concentrations (hyperbilirubinemia). Thus, the BV/BR redox cycle that is controlled by BLVRB can play important roles in ROS regulation.[18] Furthermore, it has been shown that induced pluripotent stem cells (iPSCs) expressing a loss-of-function mutant of BLVRB ($BLVRB^{S111L}$) accumulate ROS and a significantly increased proliferation (measured by MK-colony-forming: CFU-MK) was also identified in the modified $CD34^+/BLVRB^{S111L}$ hematopoietic stem cells (HSCs), while wild-type BLVRB does not have either of the two effects.[14] The loss-of-function mutant ($BLVRB^{S111L}$) induces MK differentiation and hence more platelets by ROS accumulation.[13,19] Thus, the inhibition of BLVRB activity, that is, the removal of the antioxidant BR, represents a novel strategy to increase the platelet generation because of a unique BLVRB-specific redox-regulation in the heme degradation pathway.[14]

Received: November 18, 2021
Published: December 27, 2021

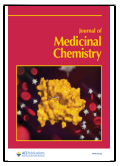

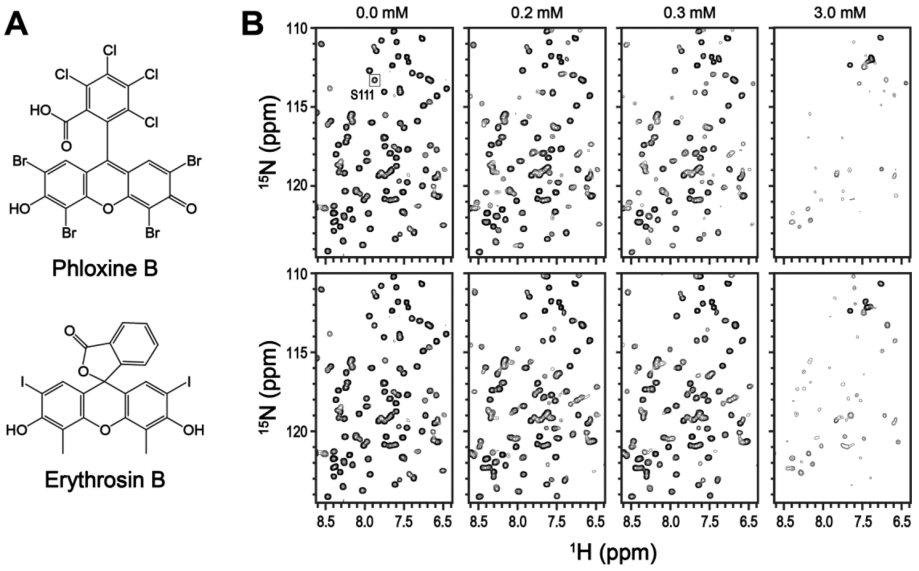

Figure 1. Multimerization of BLVRB induced by xanthene-based drug candidates. (A) Molecular structure of xanthene-based drug candidates, phloxine B and erythrosin B. (B) NMR titration experiment with phloxine B (top) and erythrosin B (bottom). Ratio 1:0, 1:0.6, 1:1, and 1:10 [Half-holo form of BLVRB (0.3 mM) : phloxine B and erythrosin B].

To achieve the inhibition of BLVRB activity, xanthene dyes and acridine-containing compounds have been derived.[20] These two compounds share structural similarity to a natural BLVRB substrate, flavin mononucleotide (FMN). Among these xanthene dyes, erythrosin B and phloxine B were found to be the two most potent inhibitors.[21,22] Molecular modeling and X-ray crystallographic studies showed that erythrosin B and phloxine B bind to the active site of BLVRB.[22] In addition, the hydrogen bond network in the active site of BLVRB and the critical role of the S111 residue for the catalytic activity were also elucidated.[23−25] Interestingly, Lineweaver−Burk plot analyses showed that these compounds inhibit the activity in a noncompetitive manner, although they bind similarly but not as deeply in the binding pocket of BLVRB as the natural substrate, FMN, engages.[22,25,26]

Both erythrosin B and phloxine B have been used for coloring food, and the antimicrobial activity of phloxine B was also reported for various Gram-positive bacteria.[27] However, chronic administration of erythrosin B was shown to promote thyroid tumors in rats.[28] Furthermore, through careful investigation with nuclear magnetic resonance (NMR) and dynamic light scattering (DLS) experiments (see results, Figure 1, and supporting materials), we verified that erythrosin B and phloxine B induce multimerization of BLVRB, which can cause potential complications to use erythrosin B and phloxine B as therapeutics.[29] Thus, new drug candidates inhibiting BLVRB are in need for treating platelet disorders. We have chosen a drug repurposing method for screening new candidates because it has great advantages: (i) decreasing the number of clinical trial steps required can reduce the time and costs for the medicine to reach the market and (ii) facilitating the discovery of new mechanisms of action for the known and new kinds of small molecules.[30−34] The downside is that this approach is less attractive for pharmaceutical companies because in clinical practice, generic products with the same API can still be used off-label.[35] To reposition approved drugs as candidates for inhibiting BLVRB, we screened 1496 Food and Drug Administration (FDA)-approved molecules for BLVRB inhibition. We found 20 candidate molecules with IC_{50} less than 5 μM and derived their exact binding mode to the active site of BLVRB by NMR chemical shift perturbation (CSP). Detailed biophysical BLVRB-binding characteristics were evaluated for eight water-soluble candidates by isothermal titration calorimetry (ITC). Furthermore, we have determined all the eight X-ray crystal structures in complex with compounds that corroborate with the binding mode identified with the NMR studies. Our discoveries provide the action mode of potential drug candidates as a novel platform for further biological experiments and clinical trials.

2. RESULTS AND DISCUSSION

2.1. Multimerization of BLVRB Induced by Xanthene-Based Drug Candidates, Erythrosin B and Phloxine B.

Erythrosin B and phloxine B (Figure 1A) are recognized as the two most potent inhibitors of BLVRB.[22] Because the inhibition mechanism of these two compounds was investigated through in silico and crystallographic studies, we set out to investigate the inhibition mechanism in a physiological environment by NMR. As expected from the previous studies, the two compounds induced chemical shift changes of NMR resonances of BLVRB observed by two-dimensional (2D) ^{1}H-^{15}N heteronuclear single quantum correlation (HSQC), clearly indicating inhibitor binding to BLVRB. However, when the concentration of erythrosin B or phloxine B was increased, we observed that backbone amide signals disappeared, and only certain side-chain peaks remained visible (Figure 1B).

This indicates multimerization of BLVRB upon the addition of erythrosin B and phloxine B. The result is also corroborated with DLS showing an increase in the size of the BLVRB-inhibitor complex upon the concentration increase of erythrosin B or phloxine B (Figure S1).[36] Thus, the inhibition mechanism of erythrosin B and phloxine B may be due to not only blocking of the active site in BLVRB but also multimerization of BLVRB. The multimerization may cause complications to spatial control in the subcellular scale,[29] and thus, we set out to find alternative molecules by screening FDA-approved drugs without this complication.

https://doi.org/10.1021/acs.jmedchem.1c01664
J. Med. Chem. 2022, 65, 2548−2557

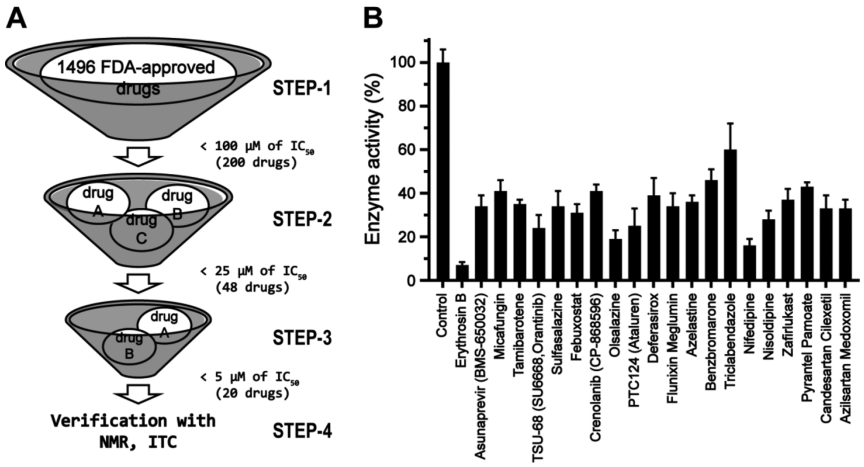

Figure 2. Effective FDA-approved drug screening through BLVRB enzyme activity assay. (A) Overview of the steps to screen FDA-approved drugs. (B) Twenty FDA-approved drugs under 5 μM of IC_{50} were selected. Normalized enzyme activity (%) was calculated by measuring NADPH decrement at 430 nm wavelength in 96-well plates. Control was measured in the absence of any drugs, and all experiments were repeated three times.

2.2. Screening FDA-Approved Drugs to Identify BLVRB Inhibitors with an Enzyme Activity Assay. For the initial screening using FDA-approved drugs, we have chosen an enzyme activity assay for BLVRB. Because BLVRB catalyzes the NAD(*P*)H-dependent reduction of FMN,[37−42] changes in the NAD(*P*)H concentration in the presence of FMN can be used to measure enzyme activity in the absence (control) and presence of drug candidates. Thus, we initially measured BLVRB enzyme activity conditions as a control and compared the level of inhibition by stepwise-measuring its activity in the presence of 1496 FDA-approved drugs (Figure S2, Supporting Information). IC_{50} was used as the selection criterion for further screenings of more potent inhibitory molecules with a lower IC_{50} value (Figure 2A). Through this procedure, we identified 20 inhibitors, where IC_{50} was lower than 5 μM (Figure 2B). To avoid false positives or assay artifacts resulting from pan-assay interference compounds (PAINS), a low critical micelle concentration (CMC) of triton X-100 was included in all enzyme activity assay buffer.[43]

As explained in the next paragraph, the binding surfaces of BLVRB for all 20 inhibitors are almost identical with those of erythrosin B and phloxine B using ^{1}H-^{15}N HSQC CSP experiments, pointing out that all 20 inhibitors bind BLVRB in the active site by replacing the FMN (Tables 1 and S1, Supporting Information). Because drugs should work in an aqueous environment for blood disorders, eight top drug candidates with the consideration of solubility were selected for further characterization using biophysical methods such as NMR and ITC.

2.3. Binding Investigation of Drug Candidates on the Substrate Pocket Using NMR Spectroscopy. Protein-based NMR spectroscopy is one of the most well-suited methods to identify intermolecular interactions, including small molecule and protein interactions. Furthermore, protein-based NMR methods provide information on binding sites, which is of prime interest for optimizing small molecules.[44,45] This is usually achieved by monitoring chemical shift changes in ^{1}H-^{15}N HSQC spectra. The assignment of amide resonances is needed to interpret the HSQC spectra. This was performed by HNCA and HN(*CO*)CA spectra (Figure S3, Supporting Information), providing 95% of the backbone resonance assignments.[46−48] Therefore, we performed HSQC experiments of ^{15}N-labeled BLVRB titrating increasing amounts of drug candidates to monitor the chemical shift changes upon the binding of the inhibitors identified in the enzyme activity assay. In particular, Ser111 was previously identified as a key residue involved in the catalytic mechanism of BLVRB. Thus, we monitored chemical shift changes of the Ser111 amide signal in HSQC spectra and found that eight FDA-approved drugs binding to BLVRB shift the amide resonances of Ser111 (Figure 3).

Using the assignment, the CSPs of BLVRB by each drug were extracted from the spectra (Figure 4) and the binding site of each drug was identified based on the CSPs (Table 1), which clearly show that the binding site is where FMN binds BLVRB.[25]

All the drug compounds except two drugs are pure, and thus, there is no doubt which compounds are the active molecules. However, two drugs were delivered as a mixture of two compounds; (i) B1445, flunixin is a potent inhibitor of the enzyme cyclooxygenase and is formulated with an excipient, meglumine. (ii) B2149, pyrantel is a pyrimidine-derivative anthelmintic agent for ascariasis, and pamoate is a counterion to increase the dissolution of pyrantel. To identify which compounds are active for inhibition, we performed water-LOGSY titration experiments[49] in the presence of BLVRB by monitoring the drug compound signals (Figure S4). Through water-LOGSY titration experiments, we could clearly identify flunixin, not meglumine, as an active compound inhibiting BLVRB (Figure S5). Interestingly, the water-LOGSY data showed that pamoate, not pyrantel, binds BLVRB more specifically, although pyrantel resembles FMN more than pamoate (Figure S5B,D). Furthermore, water-LOGSY experiments for the other six drugs confirmed that the presence of the aromatic ring structure is critical for binding to BLVRB (Figure S4, Supporting Information), indicating that the hydrophobic interactions are major driving force for the interactions between drug compounds and BLVRB. Through these results, we conclude that all eight selected FDA-approved drugs bind to the substrate-binding pocket of BLVRB and especially, Ser111, which is the most critical residue for the enzyme activity, thereby inhibiting the binding of a substrate such as FMN or biliverdin IXβ. The verification of the drug-binding effect on the BLVRB surface also successfully

https://doi.org/10.1021/acs.jmedchem.1c01664
J. Med. Chem. 2022, 65, 2548−2557

Table 1. Properties of the BLVRB Inhibitor Selected from FDA-Approved Drugs[a]

Structure	ID (Log P)	Mapping
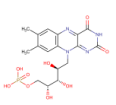	Flavin mononucleotide (-1.43)	
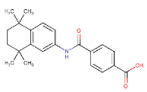	A3856 Tamibarotene (5.37)	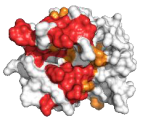
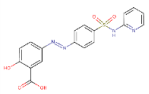	A5770 Sulfasalazine (3.90)	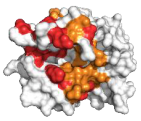
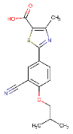	A5926 Febuxostat (3.68)	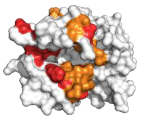
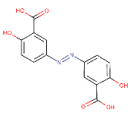	A8490 Olsalazine (-0.55)	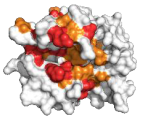
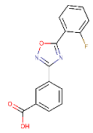	A8553 Ataluren (3.73)	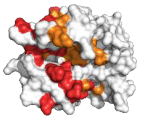
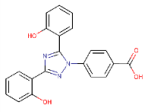	A8639 Deferasirox (4.34)	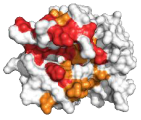
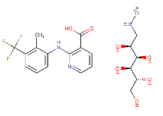	B1445 Flunixin + Meglumine (3.80)	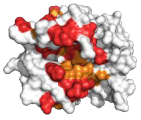
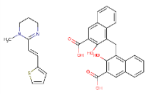	B2149 Pyrantel + Pamoate (5.52)	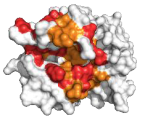

[a]In the CSP mapping (PDB: 1HE4), the residues showing strong and mild CSP are decorated with red and orange color, respectively.

performed by analyzing CSPs and mapping on the surface structure of the BLVRB clearly identified that the binding sites of all eight drug compounds are the FMN binding site, in particular, the xanthine ring of FMN.

2.4. Thermodynamic Characterization of the Screened Drug Binding to BLVRB. ITC is a method to directly measure the heat produced during complex formation at a constant temperature. The thermodynamic quantities characterizing the complex ΔH and ΔS can be characterized.[50] We determined those values for the eight top candidate drugs as well as xanthene-based compounds (erythrosin B and phloxine B) binding to BLVRB. All ITC experiments were measured at 25 °C, that is, the same temperature at which the enzyme activity and NMR experiments were performed. The dissociation constants (K_Ds) of all the screened compounds as well as the xanthene-based compounds ranged between 0.07 and 1.8 μM (Table 2; Figure S6), which are well below our activity cutoff (IC_{50} < 5 μM; Figure 1). Thus, all compounds are strong and effective binders to BLVRB.

Compared to the previously identified xanthene-based inhibitors, erythrosin B and phloxine B, all the compounds screened in this study display similar or stronger binding affinity. Particularly, olsalazine shows the strongest affinity (0.07 μM) to BLVRB among all the compounds. Furthermore, reducing the size of the compound compared to xanthene-based compounds could reduce specific interactions between BLVRB and compounds, which can be monitored through enthalpic contribution in the ITC data (Table 2). Binding of all the compounds is mostly driven by enthalpic changes (specific interactions between BLVRB and compounds), except phloxine B. In addition, two other compounds, erythrosin B and tamibarotene, display significant contribution from entropy (31 and 44% of the total binding free energy, respectively). These results may imply that the bulkiness of xanthene-based drugs (erythrosin B and phloxine B) may energetically support the binding by excluding water molecules from the binding site, which is known to increase the entropy of water. For tamibarotene, the large entropic contribution to ΔG may be explained by the conformational flexibility compared to other compounds. Interestingly, two compounds, sulfasalazine and PTC124 (ataluren), show a decrease in the binding entropy. In conclusion, the ITC results support specific interactions between BLVRB and all the eight screened drug candidates.

2.5. X-Ray Crystal Structures of BLVRB-Drug Complexes. All the eight crystal structures of BLVRB in complex with $NADP^+$ and drugs have been determined at 1.4−1.7 Å resolution (Table S2). The space groups of all the crystals, including the BLVRB-$NADP^+$ complex, were $P2_12_12$, except those of BLVRB-$NADP^+$ complexed with ataluren and pamoate ($P2_12_12_1$). All the crystal poses contained two BLVRB molecules (Mol-A and -B) in the crystal asymmetric unit (Figure S7), except ataluren and pamoate complexes that contained two pairs of BLVRB molecules (Mol-A/B and Mol-C/D) in the $P2_12_12_1$ asymmetry (Figure S8). The structure of the Mol-A/B pair is almost identical to that of the Mol-C/D pair, in which the root mean square deviation (RMSD) values of heavy atoms between two pairs were 0.148 and 0.184 Å for the ataluren and pamoate complexes, respectively. The difference between Mol-A/B and Mol-C/D likely originated from subtle differences in the orientations of several side chains around the drug-binding sites (not shown), in addition to a subtle difference in crystal packing induced by the soaking process of specific drugs. On the other hand, the Mol-A and -B display somewhat significant difference between them. The heavy-atom RMSD between Mol-A and Mol-B ranges from 1.12 to 1.25 Å for the different drug complexes (Figure S7B). One specific part of BLVRB located in the region of the crystal contacts greatly varies between the Mol-A and -B (Figure S7B, cyan circled). In particular, the structures of the drug-binding pockets show difference for Mol-A and Mol-B (Figure S7C). While the structure of the binding pocket for the drug compounds in Mol-B is affected by the second BLVRB molecule through the crystal contacts, the structure of the

https://doi.org/10.1021/acs.jmedchem.1c01664
J. Med. Chem. 2022, 65, 2548−2557

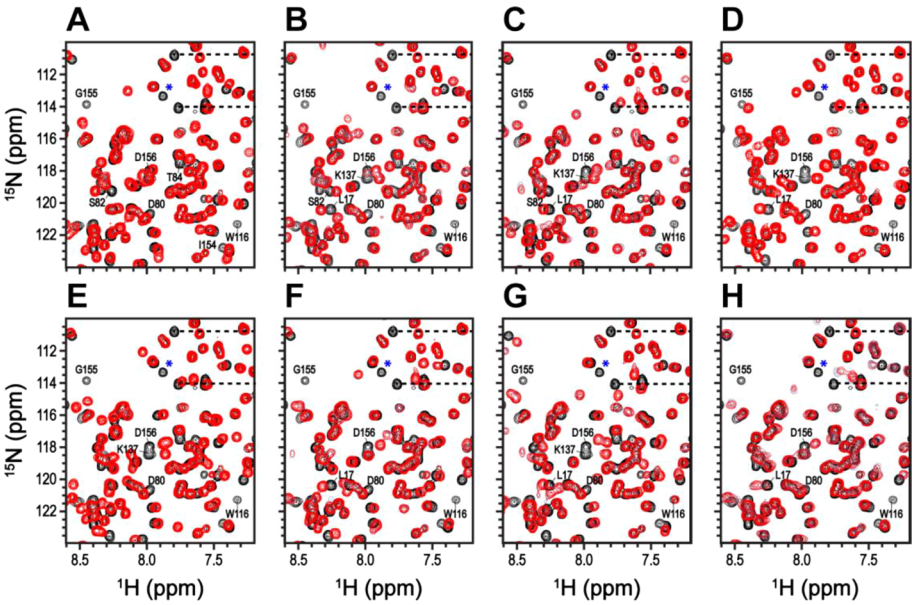

Figure 3. Portion of ^{1}H-^{15}N HSQC spectra upon ligand binding. Overlay of ^{1}H-^{15}N HSQC spectra of ^{15}N-labeled BLVRB titrated with increasing concentration of drugs: (A) tamibarotene, (B) sulfasalazine, (C) febuxostat, (D) olsalazine, (E) ataluren, (F) deferasirox, (G) flunixin+meglumine, (H) pyrantel+pamoate. Spectra are colored as follows: free protein 0.3 mM (black) and in the presence of drugs at 1 (red) molar equivalents. The Ser 111 residue that is important for enzyme activity is marked (*).

drug-binding pocket in Mol-A is well preserved with a monomeric state of BLVRB (Figure S7D). Moreover, the overlay of the Mol-A complexed with olsalazine to the Mol-B shows that its R174 residue causes a spatial collision with the D130 of the original Mol-A (Figure S7E). The comparisons of the crystal B-factors also show that the Mol-B, including the bound NADP^{+} and drug molecules, has higher B-factor values than the Mol-A (Figure S9). Thus, the detailed structural analyses of all the complexes were focused on Mol-A.

The overall structures of BLVRB in all the complexes are almost identical to the previously determined structures. For example, the backbone RMSDs of all the complexes compared to the previously resolved BLVRB-NADP^{+}-FMN complex (pdb id: 1HE4) are less than 0.3 Å, highlighting a high similarity between the structures of BLVRB in all the complexes and BLVRB complexed with its native substrate.

The binding sites of all the drug compounds are close to the nicotinamide moiety of the NADP^{+} cofactor where the xanthine ring of FMN acquires a similar pose to the xanthine-based inhibitors, phloxine B and erythrosine, as identified by the NMR titration experiments (Figure 5A). The major driving interaction for the drug compound binding is the ring stacking between the nicotinamide moiety of NADP^{+} and the drug compounds and hydrophobic interactions between BLVRB and the drug compounds composed of R78, N79, L81, S111, A112, F113, W116, L125, V128, H132, P151, P152, H153, and R174 (Figure 5B). Interaction energy analysis from molecular dynamics simulations further emphasizes the importance of the stabilizing effect provided by R174 (Figure S10). In addition, favorable interactions are provided by the positively charged residues R78, K120, R124, R170, and K178. All the drug compounds, except for fluxin, replace the side chain of W116 (as resolved in the FMN complex) and shift the side chain toward the binding pocket by about 2.5 Å. The orientation of W116 in the fluxin complex remains similar to the FMN complex. However, this change in the side-chain orientation of W116 did not show significant interaction changes between the drug compounds and BLVRB. On the other hand, the side chain of R174 shows hydrogen bonding with olsalazine and altaluren, which may increase the binding of the drug compounds. Furthermore, the orientation of R174 may increase the hydrophobic interaction between the drug compound and BLVRB. These observations corroborate well the binding affinities measured with ITC (Figure 5 and Table 2).

3. CONCLUSIONS

In summary, we successfully identified 20 novel BLVRB inhibitors with IC_{50} lower than 5 μM through enzymatic screenings of 1496 FDA-approved drug library and determined the detailed BLVRB-bindings for eight water-soluble inhibitors via biochemical and biophysical studies using NMR spectroscopy, ITC, and X-ray crystal structures. All eight inhibitors display strong and specific binding with K_D ranging from 0.07 to 1.8 μM to the substrate pocket of BLVRB. With NMR, we confirmed that the binding pocket of all the compounds is similar to the natural binding partner, FMN, and an important residue for BLVRB enzymatic activity, Ser111, is involved in all the drug compound bindings. Unlike xanthene-based inhibitors, erythrosin B and phloxine B, that could specifically bind BLVRB but cause the multimerization of BLVRB possibly causing treatment complications,[51] all the new drug candidates show only specific binding to BLVRB. Together with NMR, ITC, and crystal structures, we have also identified the mode of action of the new drug compounds. The interactions between all the drug compounds and BLVRB are the hydrophobic interactions with the ring stacking between NADP+ and the drug compounds. Furthermore, it has been shown that favorable electrostatic interactions between the drug compounds and the side chain of R174 in BRVRB can increase the binding affinity. Thus, we anticipate that newly identified inhibitors will serve as a novel platform for further in-depth studies on the effects of BLVRB on physiologically related functions such as ROS accumulation and MK differentiation.

https://doi.org/10.1021/acs.jmedchem.1c01664
J. Med. Chem. 2022, 65, 2548−2557

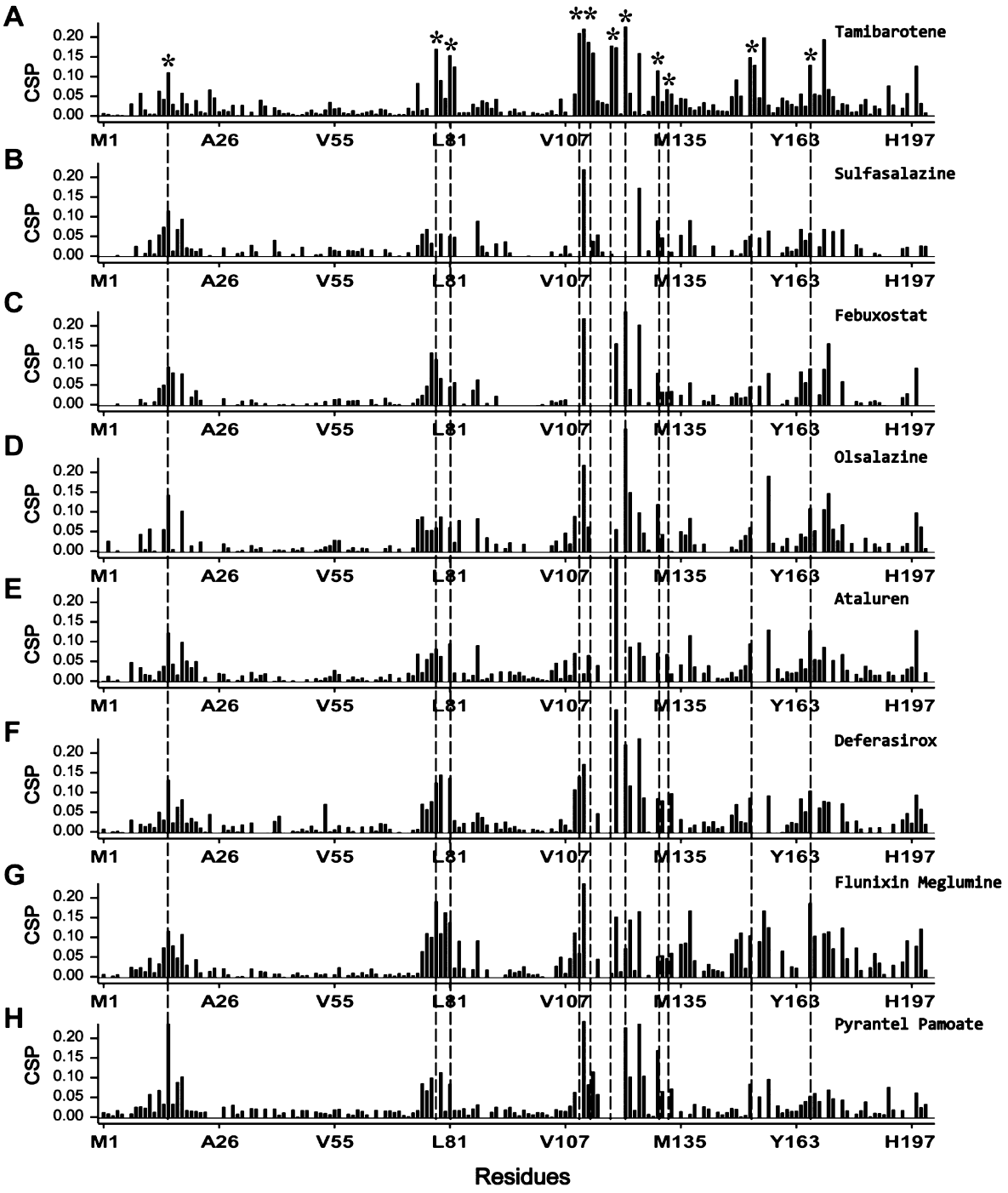

Figure 4. Binding topology of selected drugs on the substrate pocket using NMR chemical shift perturbations. Quantification of the chemical shift perturbation value of BLVRB upon binding to the identified drug. The perturbation values were obtained from the ^{1}H-^{15}N HSQC spectrum. The residues close to within 8 Å of FMN are marked (*). The order of the CSP is the same as that shown in Figure 3. (A) Tamibarotene, (B) sulfasalazine, (C) febuxostat, (D) olsalazine, (E) ataluren, (F) deferasirox, (G) flunixin+meglumine, and (H) pyrantel+pamoate.

4. EXPERIMENTAL SECTION

4.1. Materials and Chemicals. All salts, physiological buffers, FMN, NADPH, $NADP^{+}$, phloxine B, erythrosin B, and 10X PBS were purchased from Sigma Aldrich (St. Louis, MO, USA), unless otherwise specified. $^{13}C/^{15}N$ isotopes and dimethylsulfoxide (DMSO-d6) were purchased from Cambridge Isotope Laboratories. For enzymatic activity assay, 1496 FDA-approved drugs were obtained from APExBIO (Houston, Texas, USA). All FDA-approved drugs were dissolved in DMSO or DMSO-d6, and stock solutions were stored at −80 °C.

4.2. Protein Expression and Purification. The BLVRB enzyme (UniProt Accession ID: P30043) from *Homo sapiens* was cloned into an *Escherichia coli* expression vector pET21b (Novagen, Madison, WI, USA) with an N-terminal His6-tag and a thrombin cleavage site for expression in the *Escherichia coli* BL21 DE3 strain (Novagen, Madison, WI, USA). Cells were cultured at 37 °C until the cell's optical density at 600 nm reaches around 0.8; at that time, 0.5 mM isopropyl *β*-D-1-thiogalactopyranoside (IPTG) was inducted and cultured for further 18 h at 25 °C. The harvested cells were suspended in lysis buffer (pH 7.5, 50 mM Tris−HCl, 500 mM NaCl, 10 mM *β*-mercaptoethanol) with protease inhibitor cocktail (Roche) to inhibit

https://doi.org/10.1021/acs.jmedchem.1c01664
J. Med. Chem. 2022, 65, 2548−2557

Table 2. Representative ITC Data for the Binding of Each Drug to BLVRB[a]

drugs	N	ΔH (kcal/mol)	$T\Delta S$ (kcal/mol)	ΔG (kcal/mol)	K_D (μM)	pK_D (μM)
phloxine B	0.99	−3.88 ± 0.06	4.12 ± 0.12	−8.00 ± 0.10	1.36 ± 0.22	5.87 ± 0.07
erythrosin B	1.04	−6.38 ± 0.06	2.91 ± 0.13	−9.28 ± 0.11	0.16 ± 0.03	6.80 ± 0.08
tamibarotene	1.07	−4.49 ± 0.06	3.50 ± 0.10	−7.99 ± 0.08	1.38 ± 0.18	5.86 ± 0.06
sulfasalazine	0.99	−9.43 ± 0.05	−0.76 ± 0.07	−8.67 ± 0.05	0.44 ± 0.04	6.36 ± 0.04
olsalazine	0.99	−9.79 ± 0.09	0.01 ± 0.20	−9.79 ± 0.18	0.07 ± 0.02	7.15 ± 0.12
febuxostat	1.01	−5.75 ± 0.08	2.14 ± 0.11	−7.90 ± 0.08	1.63 ± 0.21	5.79 ± 0.06
ataluren (PTC124)	1.02	−10.96 ± 0.06	−1.83 ± 0.09	−9.13 ± 0.07	0.20 ± 0.02	6.70 ± 0.04
deferasirox	1.00	−7.32 ± 0.10	0.55 ± 0.12	−7.87 ± 0.07	1.71 ± 0.21	5.77 ± 0.05
flunixin + meglumine	0.99	−8.54 ± 0.04	0.41 ± 0.07	−8.95 ± 0.06	0.27 ± 0.03	6.57 ± 0.05
pyrantel + pamoate	1.01	−6.76 ± 0.13	1.08 ± 0.17	−7.84 ± 0.10	1.80 ± 0.31	5.74 ± 0.07

[a]All experiments were performed at 25 °C.

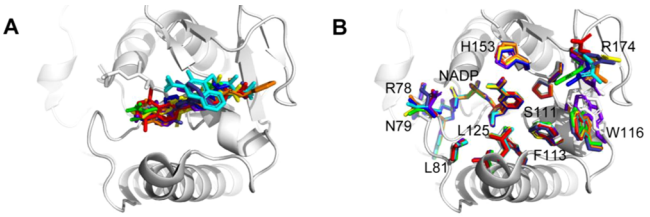

Figure 5. Binding modes of all eight drugs. (A) Overlaid eight drugs in the substrate-binding pocket of BLVRB: tamibarotene (red; PDB ID 7ER7), sulfasalazine (orange; 7ER6), febuxostat (yellow; 7ER8), olsalazine (green; 7ERA), ataluren (blue; 7ERB), deferasirox (indigo; 7ERC), flunixin (purple; 7ERD), and pamoate (cyan, 7ERE). (B) Side chains of residues in all eight structures, which are within 5 Å close to FMN, are shown in stick representation with the same color scheme as shown in Figure 5A.

protease activity, and then lysed using a sonicator [50% amplify, 2 s pulse, 10 cycles]. The HisTrap HP Ni-NTA affinity column (St. Farnsworth, Boston, USA) was applied for purification. The eluted fusion protein was cleaved overnight with 1 nm thrombin at 4 °C. At the final step, size exclusion column chromatography purification was performed using a HiLoad Superdex 75 column in the final buffer (pH 6.5, 50 mM Bis-tris, 50 mM NaCl, 1.0 mM DTT). The purity of the protein sample is over 95%. The difference between the half-holo form and the native form is whether to put $NADP^+$ before the last step or not. For NMR experiments, we prepared an isotope ^{15}N-labeled half-holo form of the BLVRB. The ^{15}N-labeled sample was used for the ^{1}H-^{15}N HSQC spectrum, and the $^{13}C/^{15}N$-labeled sample was used for HNCA and NH(*CO*)CA spectra.

4.3. Enzyme Activity Assays. The native form of BLVRB (without $NADP^+$) was used for the enzyme activity assay. The assay was performed by monitoring the rate of oxidation of NADPH at 340 nm with a Gemini EM Microplate Reader. All assays were operated at 25 °C in 100 mM phosphate-buffered saline, 0.01% of triton X-100, 100 μM FMN, 100 μM NADPH, 1 μM BLVRB and variable concentration of FDA-approved drugs. The control reactions were carried out in the absence of FDA-approved drugs to compare the effectiveness of the drug. FMN and NADPH were freshly constructed with 10 mM stock daily, calculated using an ultraviolet/visible (UV/vis) spectrometer. In each case, FMN was added to initiate the reaction and measured for 30 min. The concentration of the FDA-approved drugs was sequentially decreased in the order of 100, 25, and 5 μM to select drugs with good inhibitory effect among 1496 drugs.

4.4. NMR Titration Experiments. The half-holo form of BLVRB (with $NADP^+$) was used for NMR experiments. All FDA-approved drugs were dissolved in DMSO-d_6. NMR titration and one-dimensional (1D) experiments were operated at a ^{1}H frequency of 800 MHz using a Bruker Avance spectrometer. All experiments were performed at 298 K, and 5 mm diameter NMR tubes with a sample volume of 500 μL were used.

4.4.1. NMR Titration. The half-holo form of BLVRB samples was prepared in buffer (pH 6.5, 50 mM Bis-tris, 50 mM NaCl, 1.0 mM DTT) and dissolved in 90% H_2O and 10% D_2O. Titration experiments were executed by adding the increasing concentration of FDA-approved drugs to the half-holo form of BLVRB with the following ratios of 1:0, 1:0.5, and 1:1 [Half-holo form of BLVRB: FDA-approved drugs]. Ratios were 1:0, 1:0.6, 1:1, and 1:10 [Half-holo form of BLVRB: phloxine B and erythrosin B]. 1D spectra were recorded with water suppression using excitation sculpting with the gradient.

4.5. Isothermal Titration Calorimetry. The ITC experiment was performed using Microcal Auto-iTC200 (Malvern Instruments, UK) at 25 °C. The calorimetric cell (200 μL) contained 0.07 mM BLVRB, dissolved in buffer (pH 6.5, 50 mM Bis-Tris, 50 mM NaCl, 0.1 mM TCEP). FDA-approved drugs (0.65∼1.1 mM) in a syringe (40 μL) were titrated into BLVRB (0.07 mM). Each experiment comprised ligands that were injected 19 times with 2 μL aliquots into the 200 μL sample cell containing BLVRB (0.1 mM). $NADP^+$ mixed BLVRB concentration was calculated at 280 nm wavelength with 14,440 + 3300 M^{-1} cm^{-1} coefficient using a UV spectrometer.

Data were fitted with a nonlinear least-squares routine using a single-site binding model with the Origin software (Malvern Instruments), varying the stoichiometry (N), the enthalpy of the reaction (ΔH), the entropy of the reaction (ΔS), the Gibbs free energy of the reaction (ΔG), and the dissociation constant (K_D).

4.6. Crystallization and Structure Determination. BLVRB protein (14 mg/mL) was prepared in buffer (pH 6.5, 50 mM bis-tris, 50 mM NaCl, and 1 mM dithiothreitol), and 1 mM $NADP^+$ was added before crystallization. The initial crystallization screenings of BLVRB were performed using a Mosquito Crystallization robot (TTP LabTech) to set up the sitting drops composed of 0.2 μL of protein solution mixed with an equal volume of reservoir solution equilibrated against 100 μL of the reservoir solution at 18 °C. After initial screening, crystals were grown using the hanging drop vapor diffusion method by mixing 1.5 μL of BLVRB protein solution and 1.5 μL of reservoir buffer containing 1.8∼2.0 M ammonium sulfate and 0.1 M bis-tris (pH 6.5). Each compound (0.2 μL) stock solution (25 mM) dissolved in 100% DMSO was added to the drop and incubated at 18 °C for 24 h, and the crystals were looped and flash-frozen in liquid nitrogen. The X-ray diffraction data were collected on the beamline-11C at Pohang Light Source II (Pohang, Korea) using a DECTRIS PILATUS 6 M detector with an oscillation of 1° and 1 s exposure per frame over a 360° range at a peak wavelength of 0.97942 Å. All data sets were integrated and scaled using the HKL-2000 program.[52] The phasing by molecular replacement (MR) was performed with the previously reported coordinate of BLVRB (PDB code, 1HE5),[25] as an initial search model. The model was improved by alternating cycles of manual model building using the Coot program[53] with refinement using the PHENIX software package.[54] The analyses and visualizations of the molecular structures were performed using the Chimera program.[55]

4.7. Molecular Dynamics Simulations. Molecular dynamics simulations of BLVRB complexed with tamibarotene, flunixin,

https://doi.org/10.1021/acs.jmedchem.1c01664
J. Med. Chem. 2022, 65, 2548−2557

deferasirox, olsalazine, ataluren, sulfasalazine, and febuxostat were performed, starting with the crystallographically resolved structures using the Gromacs 2018 simulation package.[56] For each protein−ligand complex, we ran 10 independent replicas of 10 ns each when available, considering two starting conformations separately. The topology of the protein was described by the Amber99sb*ILDN[57−59] force field. Ligands and NADP+ were represented by means of the GAFF 2.11 force field[60] and RESP partial charges, respectively.[61] The system was solvated with the TIP3P water,[62] sodium and chloride ions[63] were added to neutralize the simulation box and reach 150 mM salt concentration. Hydrogen involving bonds were constrained by means of the LINCS algorithm.[64] Electrostatic interactions were treated with the Particle mesh Ewald approach[65,66] using a 1.1 nm direct space cutoff and Fourier grid spacing of 0.1 nm. The cutoff value of 1.1 nm for the van der Waals interactions was used, and dispersion correction was applied to energy and pressure. The equations of motion were integrated by means of a stochastic dynamics integrator keeping the temperature at 298.15 K with the friction of 1.0 ps-1. The Parrinello−Rahman barostat[67] with the time constant of 2.0 ps was used to keep the pressure at 1 bar.

For the interaction energy analysis, we calculated short-range electrostatic and van der Waals interaction energies between the ligand and every protein's residue. Subsequently, we identified and depicted those interactions that exceeded 10 RT threshold in at least one of the simulated systems.

■ ASSOCIATED CONTENT

Supporting Information

The Supporting Information is available free of charge at https://pubs.acs.org/doi/10.1021/acs.jmedchem.1c01664.

Molecular structure, predicted compound binding map, and solubility of 20 selected compounds from the enzyme activity assay. Statistics of X-ray data collections and structure refinements. DLS results of BLVRB depending on the concentration of erythrosin B and phloxine B. Comparison of the inhibition level of the BLVRB enzyme activity using FDA-approved drugs with 25 and 5 μM. 2D ^{1}H-^{15}N HSQC spectrum of the half-holo form of BLVRB. Water-LOGSY titration data. ITC data for the experimental validation of the binding affinity of selected compounds. X-ray crystal structures of BLVRB-drug complexes. Surface presentation of various BLVRB complex structures. B-factor values of the solved crystal structures. Nonbonded interaction energies between the ligands and protein residues obtained from molecular dynamics simulations (PDF)

Accession Codes

Authors will release the atomic coordinates upon article publication (PDB ID: 7ER6, 7ER7, 7ER8, 7ER9, 7ERA, 7ERB, 7ERC, 7ERD, and 7ERE).

■ AUTHOR INFORMATION

Corresponding Authors

Christian Griesinger − *Department of NMR Based Structural Biology, Max Planck Institute for Biophysical Chemistry, 37077 Göttingen, Germany;* orcid.org/0000-0002-1266-4344; Email: cigr@nmr.mpibpc.mpg.de

Kyoung-Seok Ryu − *Protein Structure Research Team, Korea Basic Science Institute, Cheongju-Si, Chungcheongbuk-Do 28119, South Korea;* orcid.org/0000-0002-8422-6669; Email: ksryu@kbsi.re.kr

Donghan Lee − *Department of Medicine, James Graham Brown Cancer Center, University of Louisville, Louisville, Kentucky 40202, United States;* orcid.org/0000-0002-3971-986X; Email: donghan.lee@louisville.edu

Authors

Myeongkyu Kim − *Protein Structure Research Team, Korea Basic Science Institute, Cheongju-Si, Chungcheongbuk-Do 28119, South Korea; Department of NMR Based Structural Biology, Max Planck Institute for Biophysical Chemistry, 37077 Göttingen, Germany*

Jung-Hye Ha − *New Drug Development Center, Daegu-Gyeongbuk Medical Innovation Foundation(DGMIF), Daegu 41061, South Korea*

Joonhyeok Choi − *Protein Structure Research Team, Korea Basic Science Institute, Cheongju-Si, Chungcheongbuk-Do 28119, South Korea*

Bo-Ram Kim − *Protein Structure Research Team, Korea Basic Science Institute, Cheongju-Si, Chungcheongbuk-Do 28119, South Korea*

Vytautas Gapsys − *Department of Theoretical and Computational Biophysics, Max Planck Institute for Biophysical Chemistry, 37077 Göttingen, Germany;* orcid.org/0000-0002-6761-7780

Ko On Lee − *Protein Structure Research Team, Korea Basic Science Institute, Cheongju-Si, Chungcheongbuk-Do 28119, South Korea*

Jun-Goo Jee − *Research Institute of Pharmaceutical Sciences College of Pharmacy, Kyungpook National University, Daegu 41566, South Korea*

Kalyan S. Chakrabarti − *Division of Sciences, Krea University, Sri City, Andhra Pradesh 517646, India*

Bert L. de Groot − *Department of Theoretical and Computational Biophysics, Max Planck Institute for Biophysical Chemistry, 37077 Göttingen, Germany;* orcid.org/0000-0003-3570-3534

Complete contact information is available at: https://pubs.acs.org/10.1021/acs.jmedchem.1c01664

Author Contributions

C.G., K.S.R., and D.L. planned and led the project. M.K. did most NMR and biophysical experiments. J.C., B.R.K., and K.O.L. conducted additional protein preparations and biophysical experiments. J.H.H. and K.S.R. determined crystal structures. V.G. and BdG conducted molecular dynamics simulations and their analysis. J.G.J. and K.S.C. supported the theoretical aspect for the experiment and interpretation of the drug-binding modes. All the authors contribute to writing the manuscript. M.K. and J.H.H. contributed equally to this work.

Notes

The authors declare no competing financial interest.

■ ACKNOWLEDGMENTS

This work is supported by the KBSI internal research programs (T39632, C030130, C140130, and C130000) and the James Graham Brown Cancer Center.

■ ABBREVIATIONS

BLVRB, biliverdin IXβ reductase; NADPH, nicotinamide adenine dinucleotide phosphate; FMN, flavin mononucleotide; FDA, U.S. Food and Drug Administration; NMR, nuclear magnetic resonance; ITC, isothermal titration calorimetry; DLS, dynamic light scattering; DMSO, dimethyl sulfoxide;

MK, megakaryocyte; ROS, reactive oxygen species; HSQC, heteronuclear single quantum coherence spectroscopy

REFERENCES

(1) Patel, S. R.; Hartwig, J. H.; Italiano, J. E. The biogenesis of platelets from megakaryocyte proplatelets. *J. Clin. Investig.* **2005**, *115*, 3348−3354.

(2) Pietrzyk-Nivau, A.; Poirault-Chassac, S.; Gandrille, S.; Derkaoui, S.-M.; Kauskot, A.; Letourneur, D.; Le Visage, C.; Baruch, D. Three-dimensional environment sustains hematopoietic stem cell differentiation into platelet-producing megakaryocytes. *PLoS One* **2015**, *10*, No. e0136652.

(3) Chen, S.; Su, Y.; Wang, J. Ros-mediated platelet generation: A microenvironment-dependent manner for megakaryocyte proliferation, differentiation, and maturation. *Cell Death Dis.* **2013**, *4*, e722−e722.

(4) Sim, X.; Poncz, M.; Gadue, P.; French, D. L. Understanding platelet generation from megakaryocytes: Implications for in vitro−derived platelets. *Blood* **2016**, *127*, 1227−1233.

(5) Wang, B.; Zheng, J. Platelet generation in vivo and in vitro. *Springerplus* **2016**, *5*, 787.

(6) van der Meijden, P. E.; Heemskerk, J. W. Platelet biology and functions: New concepts and clinical perspectives. *Nat. Rev. Cardiol.* **2019**, *16*, 166−179.

(7) Almazni, I.; Stapley, R.; Morgan, N. V. Inherited thrombocytopenia: Update on genes and genetic variants which may be associated with bleeding. *Front. Cardiovasc. Med.* **2019**, *6*, 80.

(8) D'Andrea, G.; Chetta, M.; Margaglione, M. Inherited platelet disorders: Thrombocytopenias and thrombocytopathies. *Blood Transfus.* **2009**, *7*, 278−292.

(9) Balduini, C. L.; Savoia, A. Genetics of familial forms of thrombocytopenia. *Hum. Genet.* **2012**, *131*, 1821−1832.

(10) Battinelli, E.; Willoughby, S. R.; Foxall, T.; Valeri, C. R.; Loscalzo, J. Induction of platelet formation from megakaryocytoid cells by nitric oxide. *Proc. Natl. Acad. Sci. U. S. A.* **2001**, *98*, 14458−14463.

(11) Kaufman, R. M.; Djulbegovic, B.; Gernsheimer, T.; Kleinman, S.; Tinmouth, A. T.; Capocelli, K. E.; Cipolle, M. D.; Cohn, C. S.; Fung, M. K.; Grossman, B. J.; Mintz, P. D.; O'Malley, B. A.; Sesok-Pizzini, D. A.; Shander, A.; Stack, G. E.; Webert, K. E.; Weinstein, R.; Welch, B. G.; Whitman, G. J.; Wong, E. C.; Tobian, A. A.; AABB. Platelet transfusion: A clinical practice guideline from the aabb. *Ann. Intern. Med.* **2015**, *162*, 205−213.

(12) Schafer, A. I. Thrombocytosis. *N. Engl. J. Med.* **2004**, *350*, 1211−1219.

(13) Sardina, J. L.; López-Ruano, G.; Sánchez-Abarca, L. I.; Pérez-Simón, J. A.; Gaztelumendi, A.; Trigueros, C.; Llanillo, M.; Sánchez-Yagüe, J.; Hernández-Hernández, A. P22 phox-dependent nadph oxidase activity is required for megakaryocytic differentiation. *Cell Death Differ.* **2010**, *17*, 1842−1854.

(14) Wu, S.; Li, Z.; Gnatenko, D. V.; Zhang, B.; Zhao, L.; Malone, L. E.; Markova, N.; Mantle, T. J.; Nesbitt, N. M.; Bahou, W. F. Blvrb redox mutation defines heme degradation in a metabolic pathway of enhanced thrombopoiesis in humans. *Blood* **2016**, *128*, 699−709.

(15) Mori, H.; Otake, T.; Morimoto, M.; Ueba, N.; Kunita, N.; Nakagami, T.; Yamasaki, N.; Taji, S. In vitro anti-human immunodeficiency virus type 1 activity of biliverdin, a bile pigment. *Jpn. J. Cancer Res.* **1991**, *82*, 755−757.

(16) Sedlak, T. W.; Saleh, M.; Higginson, D. S.; Paul, B. D.; Juluri, K. R.; Snyder, S. H. Bilirubin and glutathione have complementary antioxidant and cytoprotective roles. *Proc. Natl. Acad. Sci. U. S. A.* **2009**, *106*, 5171−5176.

(17) Dennery, P. A. Evaluating the beneficial and detrimental effects of bile pigments in early and later life. *Front. Pharmacol.* **2012**, *3*, 115.

(18) Baranano, D. E.; Rao, M.; Ferris, C. D.; Snyder, S. H. Biliverdin reductase: A major physiologic cytoprotectant. *Proc. Natl. Acad. Sci. U. S. A.* **2002**, *99*, 16093−16098.

(19) Motohashi, H.; Kimura, M.; Fujita, R.; Inoue, A.; Pan, X.; Takayama, M.; Katsuoka, F.; Aburatani, H.; Bresnick, E. H.; Yamamoto, M. Nf-e2 domination over nrf2 promotes ros accumulation and megakaryocytic maturation. *Blood* **2010**, *115*, 677−686.

(20) Prasher, P.; Sharma, M. Medicinal chemistry of acridine and its analogues. *MedChemComm* **2018**, *9*, 1589−1618.

(21) Duarte, P.; Ferreira, D. P.; Ferreira Machado, I.; Vieira Ferreira, L. F.; Rodríguez, H. B.; San Román, E. Phloxine b as a probe for entrapment in microcrystalline cellulose. *Molecules* **2012**, *17*, 1602−1616.

(22) Nesbitt, N. M.; Zheng, X.; Li, Z.; Manso, J. A.; Yen, W. Y.; Malone, L. E.; Ripoll-Rozada, J.; Pereira, P. J. B.; Mantle, T. J.; Wang, J.; Bahou, W. F. In silico and crystallographic studies identify key structural features of biliverdin ixbeta reductase inhibitors having nanomolar potency. *J. Biol. Chem.* **2018**, *293*, 5431−5446.

(23) Chu, W. T.; Nesbitt, N. M.; Gnatenko, D. V.; Li, Z.; Zhang, B.; Seeliger, M. A.; Browne, S.; Mantle, T. J.; Bahou, W. F.; Wang, J. Enzymatic activity and thermodynamic stability of biliverdin ixbeta reductase are maintained by an active site serine. *Chemistry* **2017**, *23*, 1891−1900.

(24) Paukovich, N.; Xue, M.; Elder, J. R.; Redzic, J. S.; Blue, A.; Pike, H.; Miller, B. G.; Pitts, T. M.; Pollock, D. D.; Hansen, K.; D'Alessandro, A.; Eisenmesser, E. Z. Biliverdin reductase b dynamics are coupled to coenzyme binding. *J. Mol. Biol.* **2018**, *430*, 3234−3250.

(25) Pereira, P. J. B.; Macedo-Ribeiro, S.; Párraga, A.; Pérez-Luque, R.; Cunningham, O.; Darcy, K.; Mantle, T. J.; Coll, M. Structure of human biliverdin ixβ reductase, an early fetal bilirubin ixβ producing enzyme. *Nat. Struct. Biol.* **2001**, *8*, 215−220.

(26) Lineweaver, H.; Burk, D. The determination of enzyme dissociation constants. *J. Am. Chem. Soc.* **1934**, *56*, 658−666.

(27) Rasooly, R. Expanding the bactericidal action of the food color additive phloxine b to gram-negative bacteria. *FEMS Immunol. Med. Microbiol.* **2005**, *45*, 239−244.

(28) Jennings, A. S.; Schwartz, S. L.; Balter, N. J.; Gardner, D.; Witorsch, R. J. Effects of oral erythrosine (2′, 4′, 5′, 7′-tetraiodofluorescein) on the pituitary-thyroid axis in rats. *Toxicol. Appl. Pharmacol.* **1990**, *103*, 549−556.

(29) Ballister, E. R. *Inducible protein dimerization: New tools and applications to understanding the mitotic checkpoint*; University of Pennsylvania, 2014.

(30) Ashburn, T. T.; Thor, K. B. Drug repositioning: Identifying and developing new uses for existing drugs. *Nat. Rev. Drug Discovery* **2004**, *3*, 673−683.

(31) Novac, N. Challenges and opportunities of drug repositioning. *Trends Pharmacol. Sci.* **2013**, *34*, 267−272.

(32) Sleigh, S. H.; Barton, C. L. Repurposing strategies for therapeutics. *Pharm. Med.* **2010**, *24*, 151−159.

(33) Rosa, S. G. V.; Santos, W. C. Clinical trials on drug repositioning for covid-19 treatment. *Rev. Panam. Salud Pública* **2020**, *44*, No. e40.

(34) Stumpf, W. E. *Drug localization in tissues and cells*; IDDC-Press; Chapel Hill, NC, 2003.

(35) Johnson, J. R.; Samuels, P. Review of autoimmune thrombocytopenia: Pathogenesis, diagnosis, and management in pregnancy. *Clin. Obstet. Gynecol.* **1999**, *42*, 317−326.

(36) Lorber, B.; Fischer, F.; Bailly, M.; Roy, H.; Kern, D. Protein analysis by dynamic light scattering: Methods and techniques for students. *Biochem. Mol. Biol. Educ.* **2012**, *40*, 372−382.

(37) Mack, C. P.; Hultquist, D. E.; Shlafer, M. Myocardial flavin reductase and riboflavin: A potential role in decreasing reoxygenation injury. *Biochem. Biophys. Res. Commun.* **1995**, *212*, 35−40.

(38) Shalloe, F.; Elliott, G.; Ennis, O.; Mantle, T. J. Evidence that biliverdin-ix beta reductase and flavin reductase are identical. *Biochem. J.* **1996**, *316*, 385−387.

(39) Cunningham, O.; Dunne, A.; Sabido, P.; Lightner, D.; Mantle, T. J. Studies on the specificity of the tetrapyrrole substrate for human biliverdin-ixalpha reductase and biliverdin-ixbeta reductase. Structure-activity relationships define models for both active sites. *J. Biol. Chem.* **2000**, *275*, 19009−19017.

https://doi.org/10.1021/acs.jmedchem.1c01664
J. Med. Chem. 2022, 65, 2548−2557

(40) Cunningham, O.; Gore, M. G.; Mantle, T. J. Initial-rate kinetics of the flavin reductase reaction catalysed by human biliverdin-ixbeta reductase (bvr-b). *Biochem. J.* **2000**, *345*, 393−399.
(41) Xu, F.; Mack, C. P.; Quandt, K. S.; Shlafer, M.; Massey, V.; Hultquist, D. E. Pyrroloquinoline quinone acts with flavin reductase to reduce ferryl myoglobin in vitro and protects isolated heart from re-oxygenation injury. *Biochem. Biophys. Res. Commun.* **1993**, *193*, 434−439.
(42) Lok, C.-N.; Lai, Y.-T.; Fung, Y.-M. Biliverdin reductase b/flavin reductase (blvrb/flr) exhibits heme-regulated, nadph-dependent reductase activity and confers cytoprotection in developing erythroid cells. *Experiment. Hematol.* **2019**, *76*, S76.
(43) Dahlin, J. L.; Nissink, J. W. M.; Strasser, J. M.; Francis, S.; Higgins, L.; Zhou, H.; Zhang, Z.; Walters, M. A. Pains in the assay: Chemical mechanisms of assay interference and promiscuous enzymatic inhibition observed during a sulfhydryl-scavenging HTS. *J. Med. Chem.* **2015**, *58*, 2091−2113.
(44) Maity, S.; Gundampati, R. K.; Suresh Kumar, T. K. Nmr methods to characterize protein-ligand interactions. *Nat. Prod. Commun.* **2019**, *14*, No. 1934578X19849296.
(45) Zuiderweg, E. R. Mapping protein− protein interactions in solution by NMR spectroscopy. *Biochemistry* **2002**, *41*, 1−7.
(46) Farmer, B.; Venters, R.; Spicer, L.; Wittekind, M.; Müller, L. A refocused and optimized HNCA: Increased sensitivity and resolution in large macromolecules. *J. Biomol. NMR* **1992**, *2*, 195−202.
(47) Grzesiek, S.; Bax, A. Improved 3d triple-resonance NMR techniques applied to a 31 kDa protein. *J. Magn. Reson. 1969* **1992**, *96*, 432−440.
(48) Kay, L. E.; Ikura, M.; Tschudin, R.; Bax, A. Three-dimensional triple-resonance NMR spectroscopy of isotopically enriched proteins. *J. Magn. Reson. 1969* **1990**, *89*, 496−514.
(49) Geist, L.; Mayer, M.; Cockcroft, X.-L.; Wolkerstorfer, B.; Kessler, D.; Engelhardt, H.; McConnell, D. B.; Konrat, R. Direct NMR probing of hydration shells of protein ligand interfaces and its application to drug design. *J. Med. Chem.* **2017**, *60*, 8708−8715.
(50) Du, X.; Li, Y.; Xia, Y.-L.; Ai, S.-M.; Liang, J.; Sang, P.; Ji, X.-L.; Liu, S.-Q. Insights into protein−ligand interactions: Mechanisms, models, and methods. *Int. J. Mol. Sci.* **2016**, *17*, 144.
(51) Sharma, A.; Slaughter, A.; Jena, N.; Feng, L.; Kessl, J. J.; Fadel, H. J.; Malani, N.; Male, F.; Wu, L.; Poeschla, E.; Bushman, F. D.; Fuchs, J. R.; Kvaratskhelia, M. A new class of multimerization selective inhibitors of hiv-1 integrase. *PLoS Pathog.* **2014**, *10*, No. e1004171.
(52) Otwinowski, Z.; Minor, W. [20] processing of x-ray diffraction data collected in oscillation mode. *Methods Enzymol.* **1997**, *276*, 307−326.
(53) Emsley, P.; Lohkamp, B.; Scott, W. G.; Cowtan, K. Features and development of coot. *Acta Crystallogr., Sect. D: Biol. Crystallogr.* **2010**, *66*, 486−501.
(54) Adams, P. D.; Afonine, P. V.; Bunkóczi, G.; Chen, V. B.; Davis, I. W.; Echols, N.; Headd, J. J.; Hung, L.-W.; Kapral, G. J.; Grosse-Kunstleve, R. W.; McCoy, A. J.; Moriarty, N. W.; Oeffner, R.; Read, R. J.; Richardson, D. C.; Richardson, J. S.; Terwilliger, T. C.; Zwart, P. H. Phenix: A comprehensive python-based system for macromolecular structure solution. *Acta Crystallogr., Sect. D: Biol. Crystallogr.* **2010**, *66*, 213−221.
(55) Pettersen, E. F.; Goddard, T. D.; Huang, C. C.; Couch, G. S.; Greenblatt, D. M.; Meng, E. C.; Ferrin, T. E. UCSF chimera—a visualization system for exploratory research and analysis. *J. Comput. Chem.* **2004**, *25*, 1605−1612.
(56) Abraham, M. J.; Murtola, T.; Schulz, R.; Páll, S.; Smith, J. C.; Hess, B.; Lindahl, E. Gromacs: High performance molecular simulations through multi-level parallelism from laptops to supercomputers. *SoftwareX* **2015**, *1-2*, 19−25.
(57) Hornak, V.; Abel, R.; Okur, A.; Strockbine, B.; Roitberg, A.; Simmerling, C. Comparison of multiple amber force fields and development of improved protein backbone parameters. *Proteins: Struct., Funct., Bioinf.* **2006**, *65*, 712−725.
(58) Best, R. B.; Hummer, G. Optimized molecular dynamics force fields applied to the helix− coil transition of polypeptides. *J. Phys. Chem. B* **2009**, *113*, 9004−9015.
(59) Lindorff-Larsen, K.; Piana, S.; Palmo, K.; Maragakis, P.; Klepeis, J. L.; Dror, R. O.; Shaw, D. E. Improved side-chain torsion potentials for the amber ff99sb protein force field. *Proteins: Struct., Funct., Bioinf.* **2010**, *78*, 1950−1958.
(60) Wang, J.; Wolf, R. M.; Caldwell, J. W.; Kollman, P. A.; Case, D. A. Development and testing of a general amber force field. *J. Comput. Chem.* **2004**, *25*, 1157−1174.
(61) Bayly, C. I.; Cieplak, P.; Cornell, W.; Kollman, P. A. A well-behaved electrostatic potential based method using charge restraints for deriving atomic charges: The resp model. *J. Phys. Chem.* **1993**, *97*, 10269−10280.
(62) Jorgensen, W. L.; Chandrasekhar, J.; Madura, J. D.; Impey, R. W.; Klein, M. L. Comparison of simple potential functions for simulating liquid water. *J. Chem. Phys.* **1983**, *79*, 926−935.
(63) Joung, I. S.; Cheatham, T. E., III Determination of alkali and halide monovalent ion parameters for use in explicitly solvated biomolecular simulations. *J. Phys. Chem. B* **2008**, *112*, 9020−9041.
(64) Hess, B.; Bekker, H.; Berendsen, H. J.; Fraaije, J. G. Lincs: A linear constraint solver for molecular simulations. *J. Comput. Chem.* **1997**, *18*, 1463−1472.
(65) Darden, T.; York, D.; Pedersen, L. Particle mesh Ewald: An n·log (n) method for Ewald sums in large systems. *J. Chem. Phys.* **1993**, *98*, 10089−10092.
(66) Essmann, U.; Perera, L.; Berkowitz, M. L.; Darden, T.; Lee, H.; Pedersen, L. G. A smooth particle mesh Ewald method. *J. Chem. Phys.* **1995**, *103*, 8577−8593.
(67) Parrinello, M.; Rahman, A. Polymorphic transitions in single crystals: A new molecular dynamics method. *J. Appl. Phys.* **1981**, *52*, 7182−7190.

https://doi.org/10.1021/acs.jmedchem.1c01664
J. Med. Chem. 2022, 65, 2548−2557